BeamDyn: A High-Fidelity Wind Turbine Blade Solver in the FAST Modular Framework

Qi Wang*[1], Nick Johnson†[2], Michael A. Sprague‡[1] and Jason Jonkman§[1]

[1]National Renewable Energy Laboratory, Golden, CO 80401
[2]Colorado School of Mines, Golden, CO 80401

BeamDyn, a Legendre-spectral-finite-element implementation of geometrically exact beam theory (GEBT), is developed to meet the design challenges associated with highly flexible composite wind turbine blades. In this paper, the governing equations of GEBT are reformulated into a nonlinear state-space form to support its coupling within the modular framework of the FAST wind turbine computer-aided-engineering (CAE) tool. Different time integration schemes (implicit and explicit) are implemented and examined for wind turbine analysis. Numerical examples are presented to show the capability of this new beam solver. A validation example of a realistic wind turbine blade CX-100 is also presented. Some practical procedures on modeling wind turbines are discussed.

I. Introduction

Wind power installations in the U.S. have exceeded 60 GW, and have become an increasingly important part of the overall energy portfolio. In recent years, the size of wind turbines has also increased in the quest for economies of scale. Larger wind turbine blades result in structures that are highly flexible. To ensure the performance and reliability of wind turbines, it is crucial to make use of computer-aided-engineering (CAE) tools that are capable of analyzing wind turbine blades in an accurate and efficient manner. Although modern computers enable three-dimensional (3D) analysis of a fully resolved blade, such analyses are too expensive for iterative design. More importantly, composite wind turbine blades are well represented as nonlinear beam models, which can capture with high-fidelity the deformation response under realistic operating conditions, and in a small fraction of the time required by a fully resolved 3D simulation.

Beam models are widely used to analyze structures that have one of its dimensions being much larger than the other two. Many engineering structures are modeled as beams, e.g., bridges, joists, and helicopter rotor blades. Similarly, beam models are well suited to analyze, with high fidelity, wind turbine blades, towers, and shafts. Most wind turbine blades are constructed of composite materials, and analysis of composite beams is more complicated than isotropic beams due to the elastic coupling effects. The geometrically exact beam theory (GEBT), first proposed by Reissner[1], is a beam-deformation model capable of enabling efficient analysis of highly flexible composite structures. GEBT has demonstrated its efficacy in helicopter rotor analysis[2]. Simo[3] and Simo and Vu-Quoc[4] extended Reissner's initial work to include 3D dynamic problems. Jelenić and Crisfield[5] derived a finite-element (FE) method that interpolates the rotation field thereby preserving the geometric exactness of this theory. It is noted that Ibrahimbegović and his colleagues implemented this theory for static[6] and dynamic[7] analysis. Readers are referred to Hodges[8], where comprehensive derivations and discussions on nonlinear composite-beam theories can be found. Recently, a mixed FE formulation of GEBT along with the numerical implementation was presented by Yu and Blair[9].

FAST is a CAE tool developed by the National Renewable Energy Laboratory (NREL) for the purposes of wind turbine analysis for both land-based and offshore wind turbines using realistic operating conditions. The current beam model in FAST is not capable of predictive analysis of highly flexible composite wind turbine blades. Recently, FAST has been reformulated under a new modularized framework that provides a rigorous means by which various mathematical systems are implemented in distinct modules and are interconnected to solve for the global, coupled, dynamic response of wind turbines and wind plants[10,11].

In this paper, a three-dimensional displacement-based implementation of the geometrically exact beam theory using Legendre spectral finite elements is presented. The theory is reformulated in a nonlinear state-space form for the purpose of integrating with the FAST framework, thereby introducing an optional high-fidelity beam model as an alternative to the current beam model. This work builds on previous efforts that showed the implementation GEBT and

*Research Engineer, National Wind Technology Center, AIAA Senior Member. Email: Qi.Wang2@nrel.gov
†Graduate Research Assistant, Department of Mechanical Engineering.
‡Senior Research Scientist, Computational Science Center.
§Senior Engineer, National Wind Technology Center.

spatial discretization executed using Legendre spectral finite elements (LSFEs)[12–15] for analysis of composite wind turbine blades. The paper is organized as follows. First, the theoretical foundation of the geometrically exact beam theory along with the reformulation of the governing equations into a state-space form is introduced. Coupling to the FAST framework is then discussed. Finally, numerical examples are provided to verify and validate the accuracy and efficiency of the present model for composite wind turbine blades.

II. Geometrically Exact Beam Theory

This section reviews the geometric exact beam theory for completeness of this paper. The content of this section can be found in many other papers and textbooks. Figure 1 shows a beam in its initial undeformed and deformed states. A reference frame $\mathbf{b}_i$ is introduced along the beam axis for the undeformed state; a frame $\mathbf{B}_i$ is introduced along each point of the deformed beam axis. Curvilinear coordinate x_1 defines the intrinsic parameterization of the reference line. In this paper, we use matrix notation to denote vectorial or vectorial-like quantities. For example, we

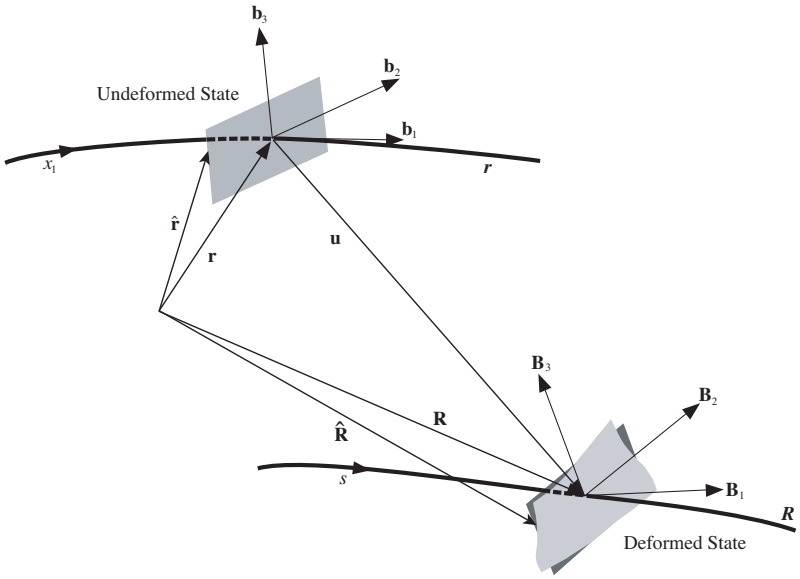

Figure 1: Schematic of beam deformation

use a underline to denote a vector $\underline{u}$, a bar to denote unit vector $\bar{n}$, and double underline to denote a tensor $\underline{\underline{\Delta}}$. Note that sometimes the underlines only denote the dimension of the corresponding matrix. The governing equations of motion for geometric exact beam theory can be written as[16]

$$\dot{\underline{h}} - \underline{F}' = \underline{f} \tag{1}$$

$$\dot{\underline{g}} + \tilde{\dot{u}}\underline{h} - \underline{M}' + (\tilde{x}_0' + \tilde{u}')^T \underline{F} = \underline{m} \tag{2}$$

where $\underline{h}$ and $\underline{g}$ are the linear and angular momenta resolved in the inertial coordinate system, respectively; $\underline{F}$ and $\underline{M}$ are the beam's sectional forces and moments, respectively; $\underline{u}$ is the 1D displacement of the reference line; $\underline{x}_0$ is the position vector of a point along the beam's reference line; $\underline{f}$ and $\underline{m}$ are the distributed force and moment applied to the beam structure. Notation $(\bullet)'$ indicates a derivative with respect to the beam axis x_1 and $(\dot{\bullet})$ indicates a derivative with respect to time. The tilde operator $(\widetilde{\bullet})$ defines a second-order, skew-symmetric tensor corresponding to the given vector. In the literature, it is also termed as "cross-product matrix". For example,

$$\widetilde{n} = \begin{bmatrix} 0 & -n_3 & n_2 \\ n_3 & 0 & -n_1 \\ -n_2 & n_1 & 0 \end{bmatrix}$$

The constitutive equations relate the velocities to the momenta and the one-dimensional strain measures to the sectional resultants as

$$\begin{Bmatrix} \underline{h} \\ \underline{g} \end{Bmatrix} = \underline{\underline{\mathcal{M}}} \begin{Bmatrix} \underline{\dot{u}} \\ \underline{\omega} \end{Bmatrix} \tag{3}$$

$$\begin{Bmatrix} \underline{F} \\ \underline{M} \end{Bmatrix} = \underline{\underline{\mathcal{C}}} \begin{Bmatrix} \underline{\epsilon} \\ \underline{\kappa} \end{Bmatrix} \tag{4}$$

where $\underline{\underline{\mathcal{M}}}$ and $\underline{\underline{\mathcal{C}}}$ are the 6×6 sectional mass and stiffness matrices, respectively (note that they are not really tensors); $\underline{\epsilon}$ and $\underline{\kappa}$ are the 1D strains and curvatures, respectively. $\underline{\omega}$ is the angular velocity vector that is defined by the rotation tensor $\underline{\underline{R}}$ as $\underline{\omega} = axial(\dot{\underline{\underline{R}}}\,\underline{\underline{R}}^T)$. The 1D strain measures are defined as

$$\begin{Bmatrix} \underline{\epsilon} \\ \underline{\kappa} \end{Bmatrix} = \begin{Bmatrix} \underline{x}_0' + \underline{u}' - (\underline{\underline{R}}\,\underline{\underline{R}}_0)\bar{\imath}_1 \\ \underline{k} \end{Bmatrix} \tag{5}$$

where $\underline{k} = \text{axial}[(\underline{\underline{RR_0}})'(\underline{\underline{RR_0}})^T]$ is the sectional curvature vector resolved in the inertial basis and $\bar{\imath}_1$ is the unit vector along x_1 direction in the inertial basis. It is noted that the three sets of equations, including equations of motion Eq. (1) and (2), constitutive equations Eq. (3) and (4), and kinematical equations Eq. (5), provided a full mathematical description of elasticity problems.

For a displacement-based finite-element implementation, there are six degree-of-freedoms at each node: three displacement components and three rotation components. Here, we use $\underline{q}$ to denote the elemental displacement array as $\underline{q}^T = \begin{bmatrix} \underline{u}^T & \underline{p}^T \end{bmatrix}$ where $\underline{u}$ is the displacement and $\underline{p}$ is the rotation-parameter vector. The acceleration array can thus be defined as $\underline{a}^T = \begin{bmatrix} \ddot{\underline{u}}^T & \dot{\underline{\omega}}^T \end{bmatrix}$. For nonlinear finite-element analysis, the discretized form of displacement, velocity, and acceleration are written as

$$\underline{q}(x_1) = \underline{\underline{N}}\,\hat{\underline{q}} \quad \underline{q}^T = \begin{bmatrix} \underline{u}^T & \underline{p}^T \end{bmatrix} \tag{6}$$

$$\underline{v}(x_1) = \underline{\underline{N}}\,\hat{\underline{v}} \quad \underline{v}^T = \begin{bmatrix} \dot{\underline{u}}^T & \underline{\omega}^T \end{bmatrix} \tag{7}$$

$$\underline{a}(x_1) = \underline{\underline{N}}\,\hat{\underline{a}} \quad \underline{a}^T = \begin{bmatrix} \ddot{\underline{u}}^T & \dot{\underline{\omega}}^T \end{bmatrix} \tag{8}$$

where $\underline{\underline{N}}$ is the shape function matrix and $\hat{(\cdot)}$ denotes a column matrix of nodal values.

To accommodate the FAST modular framework, the governing equations (1) and (2) need to be reformulated into a state-space form. Firstly we recast these equations in compact form as

$$\underline{\mathcal{F}}^I - \underline{\mathcal{F}}^{C\prime} + \underline{\mathcal{F}}^D = \underline{\mathcal{F}}^{ext} \tag{9}$$

where $\underline{\mathcal{F}}^I, \underline{\mathcal{F}}^C$ and $\underline{\mathcal{F}}^D$, and $\underline{\mathcal{F}}^{ext}$ are the inertial forces, elastic forces, and externally applied forces, respectively; their definitions are

$$\underline{\mathcal{F}}^I = \begin{Bmatrix} \dot{\underline{h}} \\ \dot{\underline{g}} \end{Bmatrix} + \begin{bmatrix} \underline{\underline{0}} & \underline{\underline{0}} \\ \tilde{\underline{u}} & \underline{\underline{0}} \end{bmatrix} \begin{Bmatrix} \underline{h} \\ \underline{g} \end{Bmatrix} \tag{10}$$

$$\underline{\mathcal{F}}^C = \begin{Bmatrix} \underline{F} \\ \underline{M} \end{Bmatrix} \tag{11}$$

$$\underline{\mathcal{F}}^D = \begin{Bmatrix} \underline{0} \\ (\tilde{x}_0' + \tilde{u}')^T \underline{F} \end{Bmatrix} \tag{12}$$

$$\underline{\mathcal{F}}^{ext} = \begin{Bmatrix} \underline{f} \\ \underline{m} \end{Bmatrix} \tag{13}$$

Along with the constitutive equations (3) and (4), the inertial force $\underline{\mathcal{F}}^I$ can be written explicitly as

$$\begin{aligned} \underline{\mathcal{F}}^I &= \begin{Bmatrix} m\ddot{\underline{u}} + (\dot{\tilde{\omega}} + \tilde{\omega}\tilde{\omega})m\underline{\eta} \\ m\tilde{\underline{\eta}}\ddot{\underline{u}} + \underline{\underline{\varrho}}\dot{\underline{\omega}} + \tilde{\omega}\underline{\underline{\varrho}}\underline{\omega} \end{Bmatrix} \\ &= \begin{bmatrix} m\underline{\underline{I}} & m\tilde{\underline{\eta}}^T \\ m\tilde{\underline{\eta}} & \underline{\underline{\varrho}} \end{bmatrix} \begin{Bmatrix} \ddot{\underline{u}} \\ \dot{\underline{\omega}} \end{Bmatrix} + \begin{bmatrix} \underline{\underline{0}} & m\tilde{\omega}\tilde{\underline{\eta}}^T \\ \underline{\underline{0}} & \tilde{\omega}\underline{\underline{\varrho}} \end{bmatrix} \begin{Bmatrix} \underline{u} \\ \underline{\omega} \end{Bmatrix} \\ &\equiv \underline{\underline{\mathfrak{M}}}\underline{a} + \underline{\underline{\mathcal{G}}}\underline{v} \end{aligned} \tag{14}$$

where m is the mass density per unit span; $\underline{\eta}$ is the center of mass location; $\underline{\varrho}$ is the moment of inertia; $\underline{\underline{I}}$ is the identity matrix. The definitions of the acceleration vector $\underline{a}$ and velocity vector $\underline{v}$ can be found in Eq. (8) and (7), respectively. By the newly introduced matrices, the compact form of equations of motion can be rewritten as

$$\underline{\underline{\mathfrak{M}}}\,\underline{a} + f(\underline{q}, \underline{v}, t) = 0 \tag{15}$$

where

$$f(\underline{q}, \underline{v}, t) = \underline{\mathcal{F}}^F - \underline{\mathcal{F}}^{C\prime} + \underline{\mathcal{F}}^D - \underline{\mathcal{F}}^{ext} \tag{16}$$

$$\begin{aligned} \underline{\mathcal{F}}^F &= \underline{\underline{\mathcal{G}}}\underline{v} \\ &= \begin{bmatrix} \underline{\underline{0}} & m\tilde{\omega}\tilde{\underline{\eta}}^T \\ \underline{\underline{0}} & \tilde{\omega}\underline{\underline{\varrho}} \end{bmatrix} \begin{Bmatrix} \underline{u} \\ \underline{\omega} \end{Bmatrix} \end{aligned} \tag{17}$$

A weighted residual formulation will be used to enforce the the dynamic equilibrium conditions in Eq. (15)

$$\int_0^l \underline{\underline{N}}^T(\underline{\underline{\mathfrak{M}}}\underline{a} + \underline{\mathcal{F}}^F - \underline{\mathcal{F}}^{C\prime} + \underline{\mathcal{F}}^D - \underline{\mathcal{F}}^{ext})dx_1 = 0 \tag{18}$$

The above equation can be recast as

$$\underline{\underline{M}}\hat{a} = F(\underline{q}, \underline{v}, t) \tag{19}$$

where

$$\underline{\underline{M}} = \int_0^l \underline{\underline{N}}^T \underline{\underline{\mathfrak{M}}}\, \underline{\underline{N}}\, dx_1 \tag{20}$$

$$\underline{F}(\underline{q}, \underline{v}, t) = \int_0^l \underline{\underline{N}}^T(-\underline{\mathcal{F}}^F + \underline{\mathcal{F}}^{C\prime} - \underline{\mathcal{F}}^D + \underline{\mathcal{F}}^{ext})dx_1 \tag{21}$$

To derive the state-space form of the governing equations, $\underline{x}(t)$ is introduced as

$$\underline{x}(t) \equiv \begin{Bmatrix} \underline{q}(t) \\ \underline{v}(t) \end{Bmatrix} \tag{22}$$

It is noted that the second component of $\underline{x}(t)$ is not $\dot{\underline{q}}$ but $\underline{v}$ in that the angular velocity $\underline{\omega}$ cannot be calculated as time derivative of the rotation parameter $\underline{p}$. The angular velocity is related to the rotation parameter by the tangent matrix as $\omega = \underline{\underline{H}}(p)\dot{\underline{p}}$. Substituting the discretized quantities in Eqs. (6) to (8) into Eq. (22) and using the relation

$$\underline{a} = \dot{\underline{v}} = \begin{Bmatrix} \ddot{\underline{u}} \\ \dot{\underline{\omega}} \end{Bmatrix} \tag{23}$$

The state-space form can be obtained as

$$\underline{\underline{A}}\, \dot{\underline{\hat{x}}}(t) = \mathfrak{f}(\underline{\hat{x}}(t), t) \tag{24}$$

$$\underline{\hat{x}}(0) = \underline{\hat{x}}_0 \tag{25}$$

where

$$\underline{\underline{A}}(\underline{\hat{x}}(t)) = \begin{bmatrix} \underline{\underline{D}} & \underline{\underline{0}} \\ \underline{\underline{0}} & \underline{\underline{M}} \end{bmatrix} \tag{26}$$

$$\underline{\underline{D}}(\underline{\hat{x}}(t)) = \int_0^l \underline{\underline{N}}^T \begin{bmatrix} \underline{\underline{I}}_3 & \underline{\underline{0}} \\ \underline{\underline{0}} & \underline{\underline{H}} \end{bmatrix} \underline{\underline{N}}\, dx_1 \tag{27}$$

$$\mathfrak{f}(\underline{\hat{x}}(t), t) = \begin{Bmatrix} \int_0^l \underline{\underline{N}}^T \underline{v}\, dx_1 \\ \underline{F}(\underline{\hat{x}}(t), t) \end{Bmatrix} \tag{28}$$

$$\underline{\hat{x}}_0 = \begin{Bmatrix} \underline{\hat{q}}_0 \\ \underline{\hat{v}}_0 \end{Bmatrix} \tag{29}$$

It is noted that the state-space form, in Eq. (24) and (25), can be solved with any number of first-order ordinary differential equations (ODE) integrators for first-order-in-time systems.

III. Numerical Examples

A. Initially twisted/curved beams

A initial twisted beam is examined first. A straight beam ($k_2 = k_3 = 0$) with an initial twist ($k_1 \neq 0$) is shown in Figure 2. The beam is linearly twisted from 0 degree twist at the root to 90 degree at the tip, and the twist is in the positive θ_1 direction. Table 1 shows the material properties for A36 steel, the geometry, and force applied to the beam. The height and base values reported in the table are the height and base of the rectangular cross-section. The beam discretized using one 20$^{\text{th}}$-order LSFE. The results for the twisted beam are shown in Table 2 and compared to the baseline results obtained from a 3D solid ANSYS model. It can be seen that the error between the BeamDyn simulation and the ANSYS baseline solution are very close.

Next a beam with initial curvature is examined. It is clear that the initial curvature plays a major role in the distribution of the elastic forces within the beam. As such it is very important to ensure that BeamDyn is capable of modeling this effect properly. A benchmark problem for a curved beam is the case proposed by Bathe[17], and is used here for verification. Figure 3 shows the configuration of the cantilevered curved beam. The beam is in the x_1,

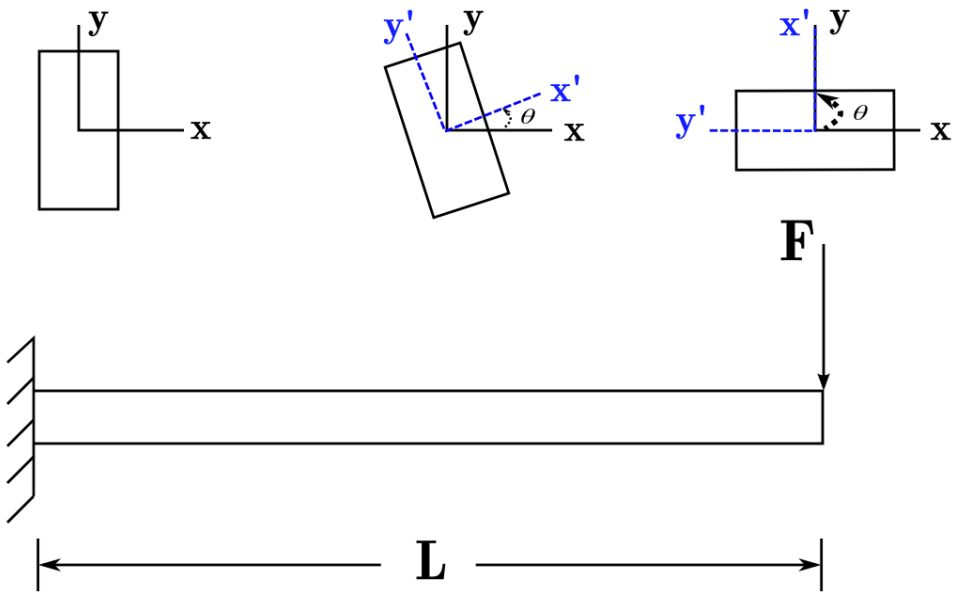

Figure 2: Sketch of a initially twisted beam

Table 1: Properties for twisted beam

Property	Value
Elastic Modulus	200 GPa
Shear Modulus	79.3 GPa
Height	0.5 m
Base	0.25 m
Length	10 m
Force	4000 kN

Table 2: Comparison of tip displacements of a initially twisted beam

	u_1 (m)	u_2 (m)	u_3 (m)
BeamDyn	-1.132727	-1.715123	-3.578671
ANSYS	-1.134192	-1.714467	-3.584232
Percent Error	0.129	0.038	0.155

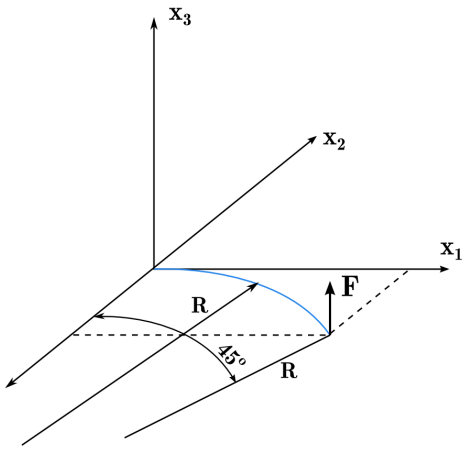

Figure 3: Sketch of a initially curveded beam

Table 3: Comparison of tip displacements of an initially curved beam

	u_1 (inch)	u_2 (inch)	u_3 (inch)
BeamDyn (one-LSFE)	-23.7	13.5	53.4
Bathe-Bolourchi [17]	-23.5	13.4	53.4

x_2 plane, and in the positive x_1 direction and negative x_2 direction. A force of 600 lbs is applied in the positive x_3 direction. The beam is defined by the 45 degree arc of a 100 inch radius centered at 100 inches in the negative x_2 direction. The geometry of the cross section for the curved beam is square, and the material properties can be found in [17]. The beam is discretized by one 5$^{\text{th}}$-order LSFE. The results for this static analysis are shown in Table 3 and compared to the results published in Bathe [17].

It can be seen from these results that the simulations from BeamDyn for a initially curved beam match quite well with the published results. Through these two numerical cases, it can therefore be said that BeamDyn is capable of modeling beams with initial twist and curvatures.

B. Static analysis of CX-100 blade

The main utility of BeamDyn will be to analyze anisotropic wind turbine blades, therefore the CX-100 will be analyzed and serve as a validation case. The CX-100 was chosen because it is a well characterized blade with a wealth of publicly available data regarding the construction and material properties of the blade. The CX-100 is a 9 m blade designed by Sandia National Laboratory [18].

The VABS cross-sectional properties for this beam were provided by Dr. D.J. Luscher of Los Alamos National Laboratory. Dr. Luscher conducted a similar study with a finite element code based on GEBT theory, called NL-Beam [19]. The cross-sectional properties were provided at 40 points along the beam. A typical stiffness matrix is shown at 2.2 m along the span of the blade, and is given by

$$C = 10^3 \times \begin{bmatrix} 193,000 & -75.4 & 12.2 & -75.2 & -1970 & -3500 \\ -75.4 & 19,500 & 4,760 & 62.6 & 67.3 & 11.3 \\ 12.2 & 4,760 & 7,210 & -450 & 17.0 & 2.68 \\ -75.2 & 62.6 & -450 & 518 & 1.66 & -1.11 \\ -1,970 & 67.3 & 17.0 & 1.66 & 2,280 & -879 \\ -3,500 & 11.6 & 2.68 & -1.11 & -875 & 4,240 \end{bmatrix}$$

Figure 4 [18] shows the different material lay-ups for the CX-100 blade. Each color represents a section with unique material properties. This figure also shows the geometry of the blade. Figure 5 [18] shows the test configuration for the static test performed at the National Wind Technology Center (NWTC) in Boulder, Colorado. The whiffle-tree configuration applies the load at 3.00 m, 5.81 m, and 7.26 m from the root of the blade to achieve a maximum root moment of 128.6 kN m. The loads and positions are given in Table 4 below.

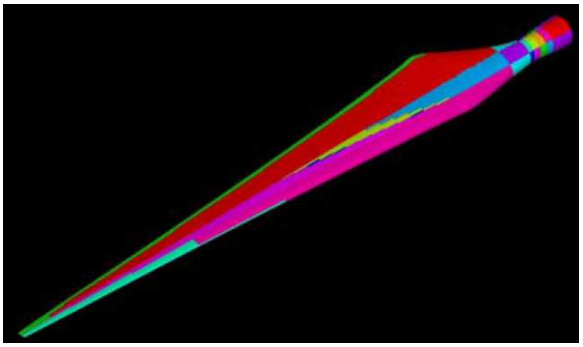

Figure 4: Material layup and geometry of CX-100 wind turbine blade [18]

The displacements, u_3, at each of the load points were tracked for the experiment and are given in Table 5. The BeamDyn simulation was completed using four 7$^{\text{th}}$-order LSFEs and the results are also given in Table 5.

The displacements are plotted in Figure 6. The maximum tip displacement for the experimental data is 1.03 m, while the maximum tip displacement for the BeamDyn simulation in 1.12 m. This discrepancy is explained in [19] as a

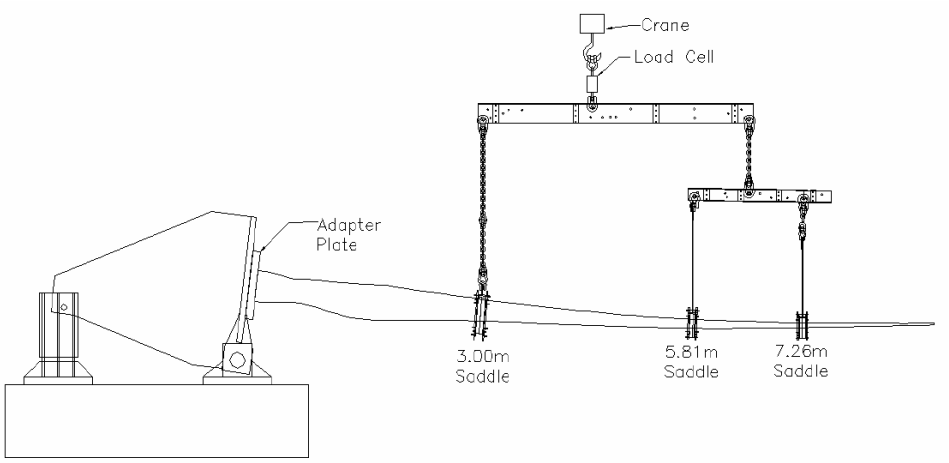

Figure 5: Test configuration for static pull test conducted at the NWTC[18]

Table 4: Positions and applied loads in CX-100 static loads test at NWTC

Saddle #	Position (m)	Applied load(kN)
1	3.00	16.9
2	5.81	5.47
3	7.26	5.59

Table 5: Experimental and BeamDyn simulation results for CX-100 static test

	u_3 at saddle #1 (m)	u_3 at saddle #2 (m)	u_3 at saddle #3 (m)
Experimental	0.083530	0.381996	0.632460
BeamDyn	0.072056	0.381074	0.698850
Percent error	13.74	0.24	10.5

difference in the rigidity of the boundary condition when calculating the 2-D sectional properties with VABS. It stands to reason that since we are using the same sectional properties the same errors would be evident, and we experience the same overall effect as the results published in [19]. It should also be noted that the tip displacement was not measured in the experiment but was extrapolated based on the recoded data at 3.00 m, 5.81 m, and 7.26 m. Overall the results are in good agreement.

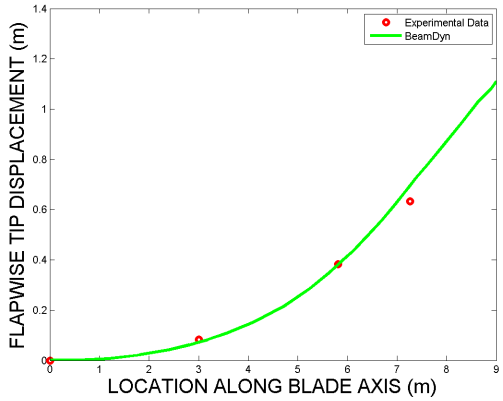

Figure 6: Displacement u_3 along the length of the blade for experimental data and BeamDyn simulation

Next a convergence study of the tip displacements is completed for the CX-100 blade in BeamDyn. Figure 7 shows the error as a function of the number of nodes. The percentage error is calculated against the experimental data in Table 5. It can be seen that the convergence rate is not exponential as desired. This is likely a function of the sharp gradients in the sectional constants. Next we mesh this blade so the element boundaries coincide with the locations where the sectional properties are defined. It was stated before that the cross-sectional properties for the CX-100 blade are given at 40 locations along the length of the blade. In order to have an element coincide with each sectional property, we must use thirty-nine LSFEs. Just as we have for the previous simulation, with two-LSFEs, the error in this simulation is found by assigning the benchmark solution as a highly refined solution in BeamDyn. Figure 8 shows the results of this simulation. Each circle on the plot indicates an additional order of the LSFE, i.e. the maximum LSFE order is six. It can be seen that we have achieved spectral convergence with this simulation, albeit with many elements. It can therefore be stated that for composite beams with sharp gradients in the cross-sectional stiffness matrix the spectral convergence is compromised. It should be noted here that while the spectral convergence suffers as a result of sharp gradients in the cross-sectional stiffness matrix the simulations still return reasonable results, so the utility of BeamDyn is not compromised in this sense.

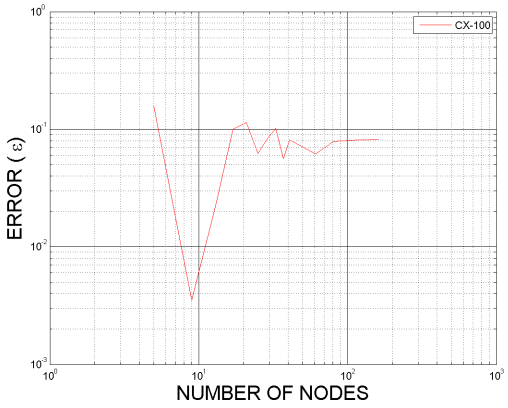

Figure 7: Error in u_3 as a function of the number of nodes

C. Dynamics of CX-100 blade

The final test case is to illustrate that BeamDyn is capable of accurately analyzing dynamic movement. Here the CX-100 blade is given a constant rotational velocity and a gravity force load is applied. A boundary condition is specified where the blade is allowed to rotate about the node located at its root. This test case is analyzed in both BeamDyn

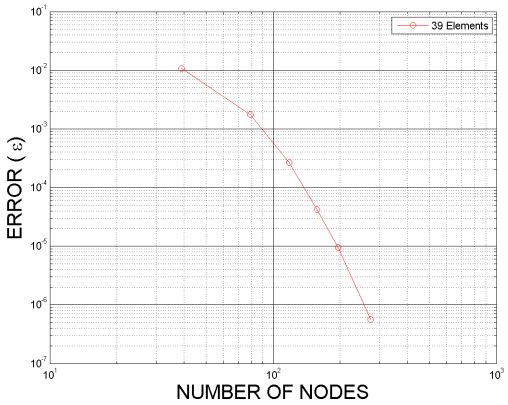

Figure 8: Error in u_3 compared to a highly refined solution in BeamDyn as a function of the number of nodes for thirty-nine 1st to 6th-order LSFEs coincident with sectional properties

and Dymore. The beam is discretized by one 8th-order element in BeamDyn, and forty 3rd-order elements in Dymore. The angular velocity of the blade is $\frac{\pi}{3}$ rad/s. The time integrator for the dynamic case is a Runge-Kutta fourth-order method, and the time step size is 5×10^{-5} s. The time integrator for Dymore is the generalized-alpha time integrator, with a time step size of 1×10^{-3} s. The total simulation time in both BeamDyn and Dymore is 6 s.

Figure 9 shows the time history for all displacements and rotations given by the BeamDyn and Dymore. For the most part the displacements are in good agreement, and the root mean square error for u_3 is 0.0335 which is given by

$$\varepsilon_{RMS} = \sqrt{\frac{\sum_{k=0}^{n_{max}} [u_3^k - u_b(t^k)]^2}{\sum_{k=0}^{n_{max}} [u_b(t^k)]^2}} \tag{30}$$

where, $u_b(t)$ is the benchmark solution and is given by the Dymore solution. Figure 10 shows the root force for the no gravity load applied and gravity load applied cases. It can be seen that the root forces are higher for the case where the gravity force is applied, as expected.

IV. Conclusion

In this paper, we reported the latest development of BeamDyn, a beam solver in FAST modularization framework. The geometrically exact beam theory has been reformulated into the first-order state-space form so first-order time integrators, as required by FAST framework, can be applied to discretize the problem in the time domain. Numerical examples are provided to validate the capability of BeamDyn against initially curved/twisted beams. A validation example is also presented where the numerical results are compared with experimental data. Good agreement can be observed. Finally, we studied the dynamic behavior of this realistic CX-100 wind turbine blade by prescribing a rotation at its root. Different time integrators are examined.

Acknowledgments

This work was supported by the U.S. Department of Energy under Contract No. DE-AC36-08-GO28308 with the National Renewable Energy Laboratory. Support was partially provided through a Laboratory Directed Research and Development grant *High-Fidelity Computational Modeling of Wind-Turbine Structural Dynamics*.

References

[1]Reissner, E., "On one-dimensional large-displacement finite-strain beam theory," *Studies in Applied Mathematics LII*, 1973, pp. 87–95.

[2]Hodges, D. H., Saberi, H., and Ormiston, R. A., "Development of Nonlinear Beam Elements for Rotorcraft Comprehensive Analyses," *Journal of the American Helicopter Society*, Vol. 52, 2007, pp. 36–48.

[3]Simo, J. C., "A finite strain beam formulation. The three-dimensional dynamic problem. Part I," *Computer Methods in Applied Mechanics and Engineering*, Vol. 49, 1985, pp. 55–70.

[4]Simo, J. C. and Vu-Quoc, L., "A three-dimensional finite-strain rod model. Part II," *Computer Methods in Applied Mechanics and Engineering*, Vol. 58, 1986, pp. 79–116.

[5]Jelenić, G. and Crisfield, M. A., "Geometrically exact 3D beam theory: implementation of a strain-invariant finite element for statics and dynamics," *Computer Methods in Applied Mechanics and Engineering*, Vol. 171, 1999, pp. 141–171.

[6]Ibrahimbegović, A., "On finite element implementation of geometrically nonlinear Reissner's beam theory: three-dimensional curved beam elements," *Computer Methods in Applied Mechanics and Engineering*, Vol. 122, 1995, pp. 11–26.

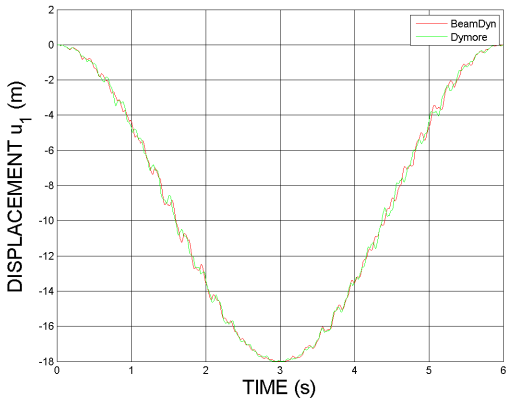

(a) u_1

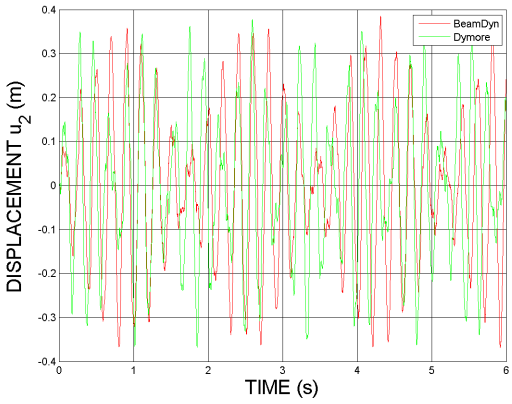

(b) u_2

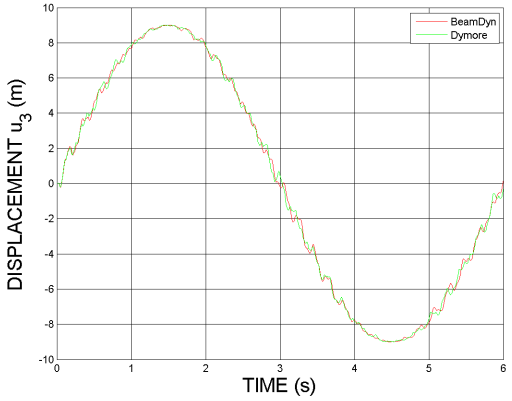

(c) u_3

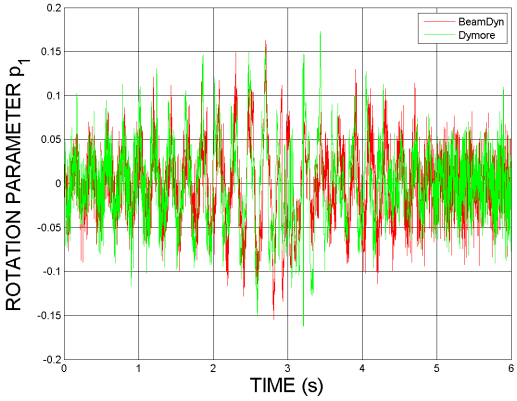

(d) p_1

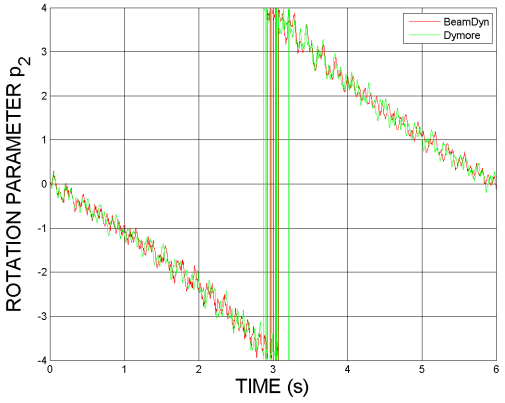

(e) p_2

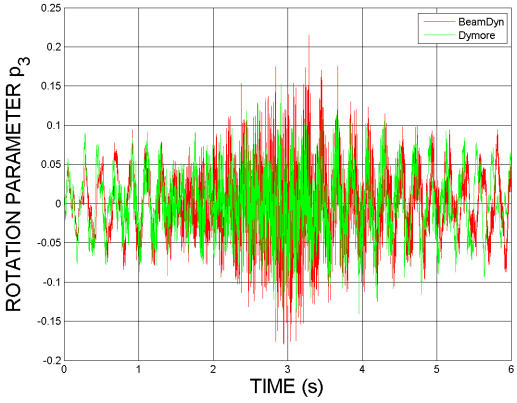

(f) p_3

Figure 9: Tip displacement and rotation histories of a CX-100 blade rotating at a constant speen

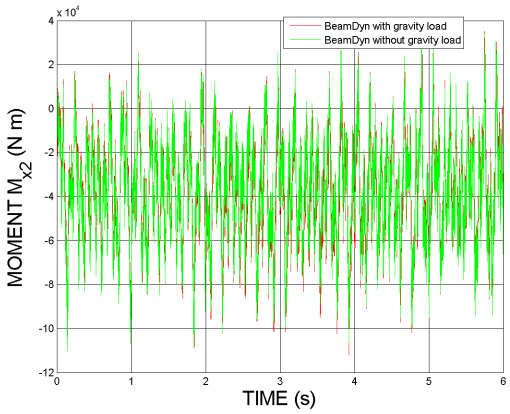

Figure 10: Root force for dynamic simulation of BeamDyn with gravity load and without gravity load

[7]Ibrahimbegović, A. and Mikdad, M. A., "Finite rotations in dynamics of beams and implicit time-stepping schemes," *International Journal for Numerical Methods in Engineering*, Vol. 41, 1998, pp. 781–814.

[8]Hodges, D. H., *Nonlinear Composite Beam Theory*, AIAA, 2006.

[9]Yu, W. and Blair, M., "GEBT: A general-purpose nonlinear analysis tool for composite beams," *Composite Structures*, Vol. 94, 2012, pp. 2677–2689.

[10]Jonkman, J. M., "The new modularization framework for the FAST wind turbine CAE tool," *Proceedings of the 51st AIAA Aerospace Sciences Meeting including the New Horizons Forum and Aerospace Exposition*, Grapevine, Texas, January 2013.

[11]Jonkman, J. and Jonkman, B., "FAST Modularization Framework," http://wind.nrel.gov/designcodes/simulators/fast/alpha/, October 2013, [Online; accessed 30-MAY-2014].

[12]Wang, Q., Yu, W., and Sprague, M. A., "Gemoetrically nonlinear analysis of composite beams using Wiener-Milenković parameters," *Proceedings of the 54th Structures, Structural Dynamics, and Materials Conference*, Boston, Massachusetts, April 2013.

[13]Wang, Q. and Sprague, M. A., "A Legendre spectral finite element implementation of geometrically exact beam theory," *Proceedings of the 54th Structures, Structural Dynamics, and Materials Conference*, Boston, Massachusetts, April 2013.

[14]Wang, Q., Sprague, M. A., Jonkman, J., and Johnson, N., "Nonlinear Legendre spectral finite elements for wind turbine blade dynamics," *Proceedings of the 32nd ASME Wind Energy Symposium*, National Harbor, Maryland, January 2014.

[15]Sprague, M. A., Jonkman, J., and Jonkman, B., "FAST modular wind turbine CAE tool: non matching spatial and temporal meshes," *Proceedings of the 32nd ASME Wind Energy Symposium*, National Harbor, Maryland, January 2014.

[16]Bauchau, O. A., *Flexible Multibody Dynamics*, Springer, 2010.

[17]Bathe, K. J. and Bolourchi, S., "Large displacement analysis of three-dimensional beam structures," *International Journal for Numerical Methods in Engineering*, Vol. 14, 1979, pp. 961–986.

[18]Paquette, J., Lairdl, D., Griffith, D., and Rip, L., "Modeling and testing of 9m research blades," *44th AIAA aerospace sciences meeting*, Vol. 19, 2006, pp. 14569–14581.

[19]Fleming, I. and Luscher, D. J., "A model for the structural dynamic response of the CX-100 wind turbine blade," *Wind Energy*, Vol. 17, 2013, pp. 877–900.